Received 4 March 2024; revised 26 March 2024; accepted 3 April 2024. Date of publication 6 May 2024; date of current version 20 May 2024.
The review of this paper was arranged by Associate Editor Amitava Chatterjee.

Digital Object Identifier 10.1109/OJIM.2024.3390197

Optimization of Electrode Configuration for 3-D Brain EIT

SIYUAN BAI [1,2], YITONG GUO [2], WEICHEN LI [3], LEI WANG [1], AND XUETAO SHI [2]

[1]Institute of Medical Research, Northwestern Polytechnical University, Xi'an 710000, China

[2]School of Biomedical Engineering, Fourth Military Medical University, Xi'an 710000, China

[3]School of Life Sciences, Northwestern University, Xi'an 710000, China

CORRESPONDING AUTHORS: L. WANG and X. SHI (e-mail: bmewanglei@nwpu.edu.cn; shixuetao@fmmu.edu.cn)

This work was supported in part by the Key Research and Development Projects of the Science and Technology Committee under Grant 2022YFC2404803; in part by the Key Basic Research Projects of the Basic Strengthening Plan of the Science and Technology Committee under Grant 2019-JCJQ-ZD-115-00-02; and in part by the Xijing Hospital Cross-Fusion Project under Grant XJZT24JC37.

(Siyuan Bai, Yitong Guo, and Weichen Li contributed equally to this work.)

ABSTRACT 3-D brain electrical impedance tomography (EIT) holds great promise for real-time noninvasive imaging of various brain injuries. However, a reference method for selecting high-performance electrode configurations has not been proposed. In this article, the optimization of electrode layout, stimulation and measurement protocols, and the number of electrodes are sequentially performed. The signal quality and image reconstruction performance of simulated perturbations in four cortical regions are evaluated with various levels of noise taken into consideration. The results showed that, considering cost and convenience, the best number of electrodes is 20, which should be placed in the suboccipital and central vertex regions as needed. Electrodes with large spacing at different heights are mainly the driving electrodes, and the potential is collected in the appropriate adjacent channels. These principles are expected to provide general guidance for the electrode configuration methods of 3-D brain EIT in clinical applications.

INDEX TERMS 3-D, brain electrical impedance tomography (EIT), electrode configurations, optimization.

I. INTRODUCTION

ELECTRICAL impedance tomography (EIT) is an imaging technique for estimating the distribution of electrical conductivity changes inside the body. It involves injecting safe currents through paired electrodes with specific patterns and measuring boundary voltages with other electrodes, followed by using algorithms to reconstruct EIT images [1]. EIT has advantages, such as high temporal resolution, low cost, real-time imaging, ease of operation, and completely noninvasive, making it a valuable complement to modern medical imaging technology [2], [3], [4]. It has shown promising applications in the diagnosis or monitoring of brain diseases, including stroke, cerebral edema, aortic arch replacement surgery, and epilepsy [5], [6], [7], [8], [9], [10]. The human brain is a volumetric conductor with a 3-D structure, and the injected current flows in all directions simultaneously. However, 2-D brain EIT has lost the conduction information outside the measurement plane.

Some authors have already considered research on 3-D brain EIT to compensate for the shortcomings of 2-D imaging in locating the depth of lesions, thus extending the application scope of brain EIT [11], [12], [13], [14].

The key to the development of 3-D brain EIT lies in determining suitable electrode configurations, including the number of electrodes, driving protocols, measurement strategies, distribution positions, etc., which is of significant importance in guiding hardware system design, improving measurement accuracy, and enhancing the quality of reconstructed images [15], [16], [17], [18]. The UCH Mk2.5 system developed by the Holder team is based on the international EEG 10-20 system, consisting of approximately three rings with 31 electrodes. Current is injected at 180° to increase current density in the center of the brain. Voltage measurements are performed along the three lines connecting the electrodes used for current injection. A total of 21 current injection pairs were used, yielding 258 measurements [19]. Subsequently,

Fabrizi tested ten current protocols on the 16-channel half-parallel system KHU Mk1, and the spiral (suboccipital) pattern achieved the best results. This protocol utilized 34 current injection pairs, including 180°, 120°, and 60° [20]. Compared to the EEG31 protocol, it demonstrated similar localization capability, suggesting its prioritized use in clinical practice. The fEITER system developed by the McCann team consisted of 32 electrodes and a total of 20 near-diametric current stimulations were designed, selecting 509 adjacent measurement values for image reconstruction [21]. Then, the number of electrodes was reduced to 16, with 45 stimulations, obtaining 540 interval measurement voltage values [22].

The specific electrode configurations used in the 3-D EIT data acquisition systems of various research teams are different. However, there is currently no research that provides relatively clear selection principles for electrode configurations for 3-D brain EIT. The following issues need to be addressed: 1) How to arrange the electrodes to improve brain EIT signal sensitivity and image quality? 2) Which is the most effective stimulation and measurement mode? and 3) What is the minimum number of electrodes required to reconstruct a reasonable EIT image that meets clinical application requirements? This article represents our contribution to these issues.

II. METHODOLOGY

The entire simulation study unfolds in three steps. Four electrode layouts and driving methods are proposed for the 32-electrode configuration initially. And the impact of measurement modes is further studied based on the comparative results. Subsequently, attempts are made to reduce the number of electrodes without significantly damaging the EIT signal and imaging quality. All simulations are conducted on a finite element human head model with a realistic structure, using a computer with 3.30-GHz CPU and 16G RAM.

A. ELECTRODE CONFIGURATION DESIGN

1) ELECTRODE LAYOUT AND STIMULATION PROTOCOL

The 3-D brain EIT systems of the McCann and Holder teams have played a significant role in multiple studies [23], [24], [25], [26]. Therefore, based on their electrode configurations, four combinations of improved layouts and stimulation methods of 32 electrode configurations are designed (Fig. 1). A current of 1 mA is injected through 20 groups of electrodes that are either nearly diametric or far apart to mitigate the scalp shunting effect. In the voltage measurements, data from electrodes that are not spatially adjacent or used for driving are rejected in the image reconstruction.

2) MEASUREMENT METHOD

The distance between measuring electrodes impacts the magnitude of the collected voltage as larger voltage values can be measured more accurately, which may be helpful in practical applications [20]. Four measurement data frames are obtained using different methods: Adjacent(AD,1-2, 2-3$\cdots$), SKIP1 (1-3, 2-4$\cdots$), SKIP2 (1-4, 2-5$\cdots$), and SKIP3 (1-5, 2-6$\cdots$) for image reconstruction.

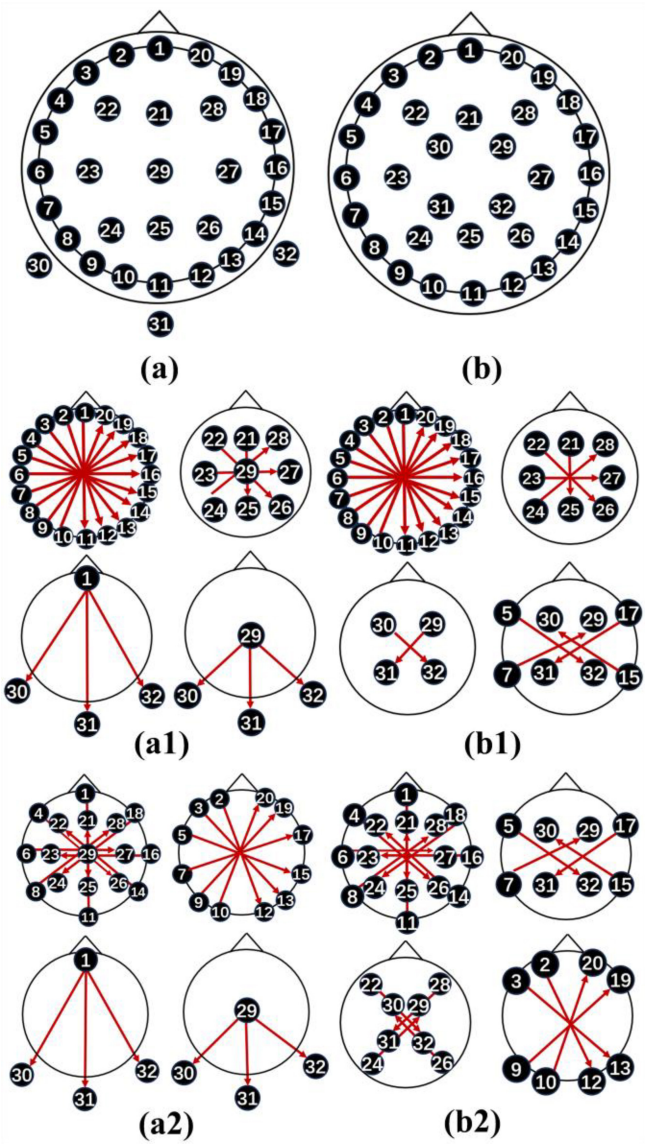

FIGURE 1. Electrode layout and stimulation schemes. (a) "Suboccipital + central vertex" layout. (b) "Triple Ring" layout. (a1) and (b1) Dominant current injection occurs between electrodes at similar heights. (a2) and (b2) Dominant current injection occurs between electrodes at different heights.

3) NUMBER OF ELECTRODES

According to the optimal arrangement, excitation, and measurement principles obtained in 2.1.1 and 2.1.2, the number of electrodes is reduced to 16 and compared with the 16-electrode configuration of the fEITER system. Based on the results, the number is then increased to 20 and 24 (Fig. 2).

B. IMAGE RECONSTRUCTION

The linear EIT image reconstruction can be represented by computing the reconstruction matrix R, which corresponds to the measurement y, in order to produce the reconstructed image x, as shown in [27]

$$x = Ry. \tag{1}$$

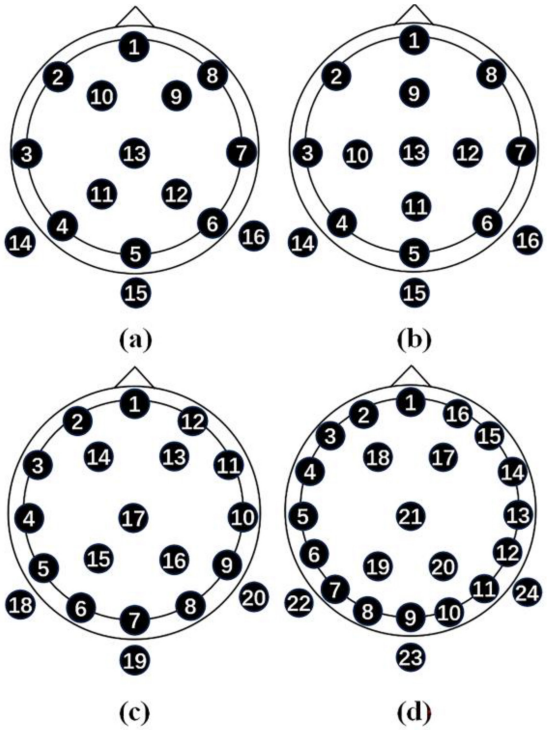

FIGURE 2. Layouts of different number of electrodes. (a) 16-I. (b) 16-II. (c) 20. (d) 24.

We use the 3-D GREIT method to calculate R, which is the best over a "training" set of measurements and images. R thus minimizes

$$\sum_k wk||tk-Ryk||2 \tag{2}$$

where t_k is the "desired image" corresponding to the training measurement frame y_k, and w_k is a weighting representing the "importance" of i in the calculation of R. Solving (2) yields

$$R = \left(\sum_k wktkyk^T\right)\left(\sum_k wkykyk^T+\gamma 2\sum n\right)-1 \tag{3}$$

where Σn is the covariance of system noise, the hyperparameter γ determines the noise performance of the reconstruction, and its value is obtained through a bisection search until the desired noise figure is achieved [28], [29].

C. SIMULATION MODEL

The forward model consists of approximately 250K elements, including scalp (0.44 S/m), skull (0.013 S/m), cerebrospinal fluid (1.78 S/m), and brain tissue (0.25 S/m) [30], [31]. The electrode diameter is 10 mm, with a contact impedance of 1 kΩ, and the grid parameterization density in the vicinity of the electrodes is enhanced [32]. Disturbance targets (1.25 S/m,10 ml) are set in the parietal, temporal, frontal, and occipital lobes, which dominate all processes of body movement and sensation. These regions should be of particular interest (Fig. 3) [33], [34], [35], [36]. The inverse model design is simplified, and modeling is conducted through fine-to-coarse mapping between different forward and inverse parameterizations. The reconstructed image consists of approximately 4K cubic voxel units, with each volume measuring approximately 10 * 10 * 10 mm^3.

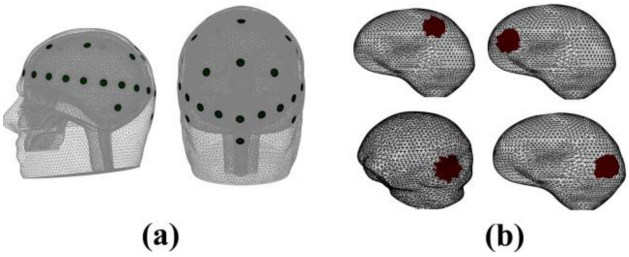

FIGURE 3. Digital models of human head and positions of cortical disturbances. (a) Finite element model with 32-electrode layout (illustrated with " Suboccipital + central vertex"). (b) Targets in the parietal lobe, frontal lobe, temporal lobe, and occipital lobe.

D. EVALUATION METRICS

To assess the quality of measurement signals and reconstructed images, four figures of merit are calculated.

1) SNR $= 20\log_{10}([\text{mean}(\text{v}i-vh)]/[\text{stdDev}(vi-vh)])$.
2) Distinguishability $= ([||vi-vh||]/[||I||])$
   where v_h and v_i are the measured voltages with and without targets in the field, and I is the amplitude of the stimulating current. A larger SNR indicates a stronger robustness of the system against noise [37]. At the same time, we aim to improve distinguishability, which makes the system more sensitive to changes in the field medium.
   The reconstructed disturbance (RP) is defined as the voxel element in the reconstructed image with conductivity changes exceeding 50% of the peak value [38].
3) *Location Error (LE):* This quantitative parameter represents the displacement of the centroid of the RP from its true target position. Ideally, it should be zero, providing accurate information about the location of the target.
4) *Volume Error (VE):* It reflects the difference between the volume of the RP and the true target. It should be small and uniform.

For the targets in the four positions, boundary voltage datasets are calculated under a noise-free condition and used for image reconstruction. Subsequently, three types of Gaussian random noise were added (with variances of 10%, 50%, and 100% of the differential signal power, denoted as N1, N2, and N3, respectively), and each subjected to five repeated simulated measurements. Under noisy conditions, the LE and VE are combined into a single general error index (GE) to evaluate the imaging quality. This index is obtained by summing the weighted contributions of the LE (weight 0.75) and the VE (weight 0.25).

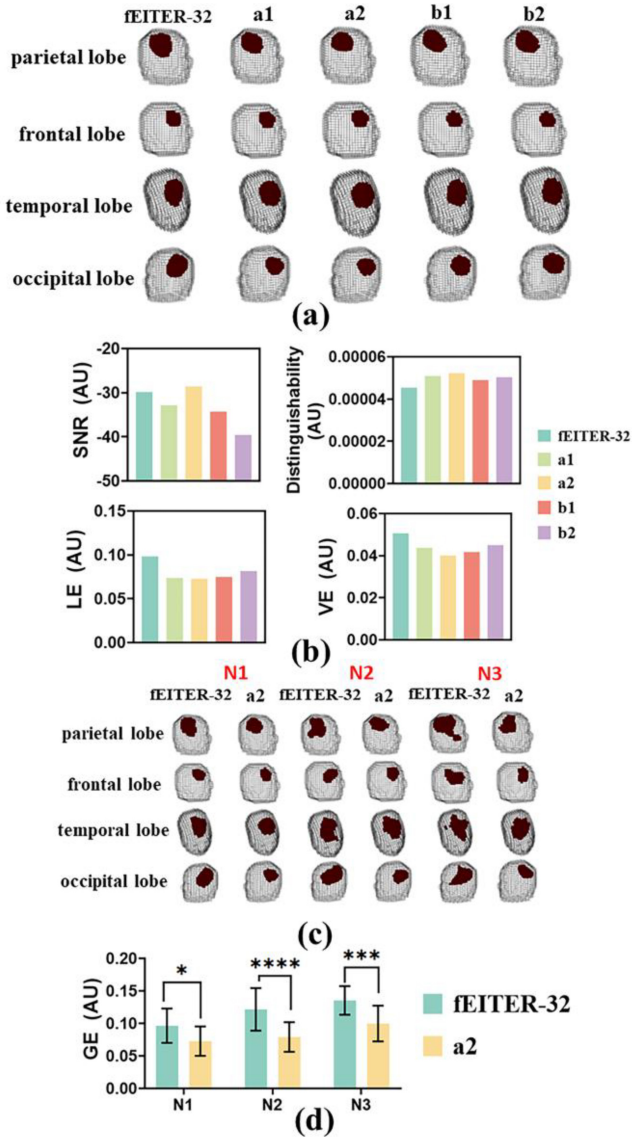

FIGURE 4. Quantitative and qualitative evaluations of different electrode layouts and driving protocols. (a) and (b) Reconstruction images and figures of merit (expressed as averages) for the five schemes without noise. (c) and (d) Reconstruction images and GE for the a2 and fEITER modes at various noise levels. (Images are presented as a 3-D model with RP. AU: Arbitrary unit.)

III. RESULTS

A. 32-ELECTRODE LAYOUT AND STIMULATION METHODS

Under the condition of no noise, the five schemes produce similar good images, with the disturbance target being positioned basically at the correct location, and no artifacts appearing elsewhere. Even for these high-quality images, all RPs are larger than the real target. The disturbances in the frontal lobe area are reconstructed more accurately. When using the a2 mode, the reconstructed targets appear more uniform overall, corresponding to the results of the quantitative assessment: the a2 mode exhibits the lowest imaging error. It also has the highest SNR and Distinguishability [Fig. 4(a) and (b)]. Under N1 noise conditions, both the fEITER mode and the a2 mode can reconstruct targets close to the correct positions. With further increase in noise, the fEITER mode fails to generate useful images, and the targets are severely distorted and obscured by noise. The imaging error of the a2 mode increases slowly, demonstrating robustness to noise, and its image quality is significantly better than that of the fEITER mode at three noise levels [Fig. 4(c) and (d)]. The a2 mode is considered an effective improvement, representing a layout and excitation strategy with superior performance.

B. MEASUREMENT METHODS

Voltage measurements are taken at different intervals in the a2 mode. Despite the presence of noise, all methods produce satisfactory images. It is evident that the SKIP modes enhance the signal's SNR and Distinguishability, albeit at the expense of a slight degradation in image quality [Fig. 5(a) and (b)]. The imaging results from the four modes under N1 and N2 noise conditions are acceptable. Conversely, in the presence of N3 noise, the RPs exhibit a high degree of inconsistency with the actual targets. Notably, there is no significant disparity in imaging performance between different measurement modes [Fig. 5(c) and (d)]. Moderately increasing the voltage measurement interval is allowed and feasible, as it takes into account the requirements of both the signal and imaging.

C. NUMBER OF ELECTRODES

Based on the layouts, excitation, and measurement principles in Sections III-A and III-B, 16-electrode configuration is designed. In the absence of noise, the fEITER mode with 45 stimulations achieves better imaging performance at all target positions, exhibiting more uniform convergence of RP, which is consistent with quantitative evaluation results. The Distinguishability also far exceeds the two types of improved modes with 20 stimulations [Fig. 6(a) and (b)]. This is expected, as the measurement data of the latter is almost halved. It can be noted that the improved modes have higher SNR, which was verified in the noise-adding experiment. Their reconstruction errors increase slowly, indicating lower sensitivity to noise compared to the fEITER mode. The imaging performance of 16-I under various noise levels is not significantly different from that of the fEITER mode. However, the images of the three schemes are severely affected by noise, and the targets cannot be effectively identified [Fig. 6(c) and (d)]. Therefore, further designs are made on 16-I to include 20 and 24 electrode configurations, with the stimulation counts increased to 26 and 32, respectively. Comparing the performance of different electrode configurations, it is found that, regardless of being affected by noise, the signal quality and imaging accuracy of the 32-electrode configuration are superior. Moreover, as the number of electrodes decreases, the reconstructed targets gradually expand. The overall performance of the 24 and 20 electrode configurations is essentially the same, with no significant increase in imaging error compared to the 32

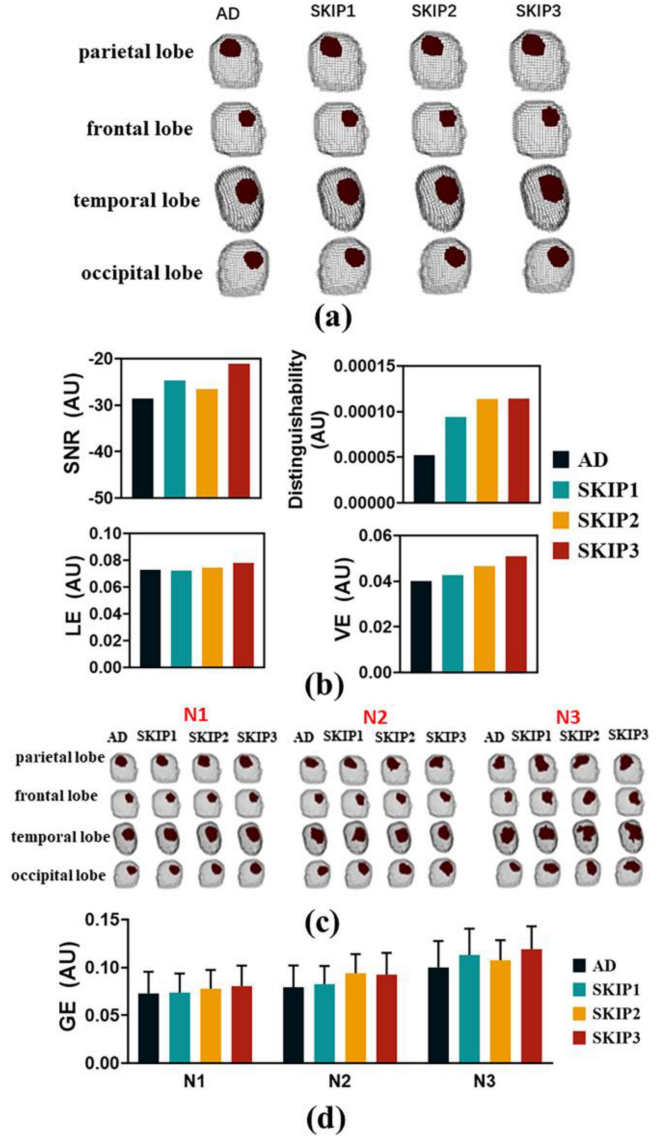

FIGURE 5. Quantitative and qualitative evaluations of four measurement modes. (a) and (b) Reconstruction images and figures of merit (expressed as averages) without noise. (c) and (d) Reconstruction images and GE at various noise levels. (Images are presented as a 3-D model with RP. AU: Arbitrary unit.)

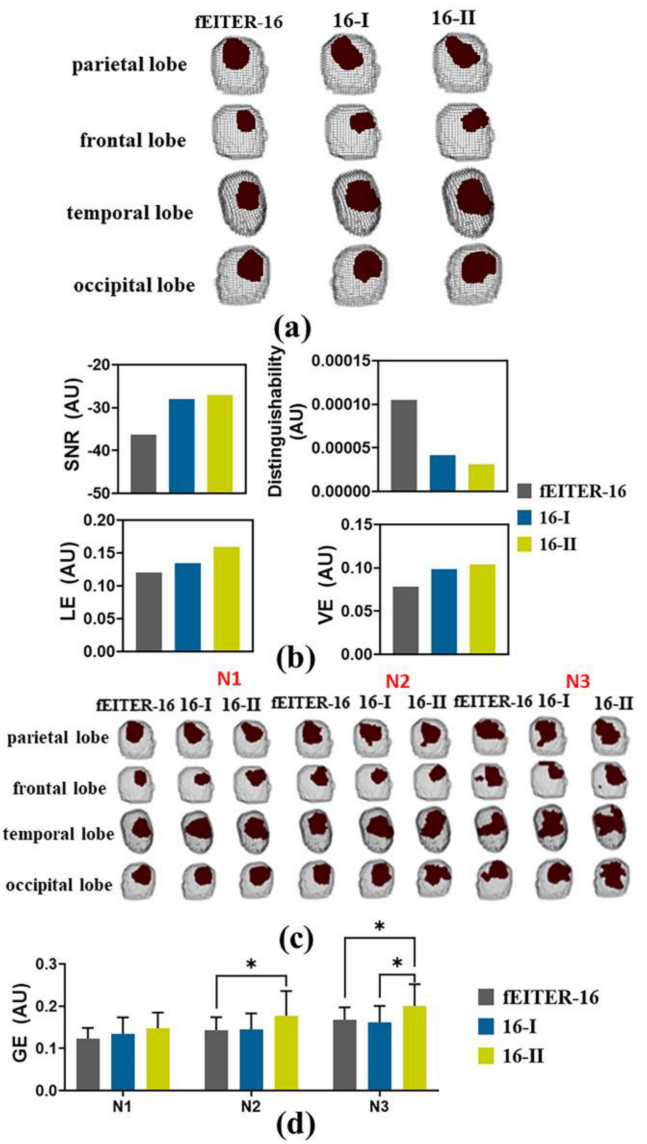

FIGURE 6. Quantitative and qualitative evaluations of three 16-electrode configurations. 16-I and 16-II mainly inject current through 20 groups of nearly diameter electrodes at different heights and obtain measurements in adjacent channels. (a) and (b) Reconstruction images and figures of merit (expressed as averages) without noise. (c) and (d) Reconstruction images and GE at various noise levels. (Images are presented as a 3-D model with RP. AU: Arbitrary unit.)

configuration. Additionally, compared to the 16-electrode configuration, there is a noticeable improvement in imaging quality (Fig. 7).

IV. DISCUSSION

The primary objective of this study is to investigate electrode configurations that are appropriate for 3-D brain EIT and to identify fundamental principles that can serve as a guide for future research. Subsequently, we aim to address three pivotal questions that we consider essential.

A. 32-ELECTRODE LAYOUT AND DRIVE PROTOCOL

Four types of electrode layouts and driving protocols are designed for two purposes. First, electrodes located at the top of the head should be given attention, as the stimulation paths dominated by them may provide more information in the vertical direction in the 3-D field. Second, to ensure comprehensive sensitivity coverage across the entire brain region, the electrodes should be uniformly distributed on the scalp surface. These considerations effectively compensate for the shortcomings of the fEITER system [21]. In Section III-A, the a2 mode demonstrated the best performance evaluation and proved to be a valuable supplement and improvement to the fEITER mode (Fig. 4). This is likely due to the variation in the injection angle of the current, which enables it to effectively reach different areas of the brain. Additionally, the use of electrodes in the suboccipital and central vertex regions could enhance

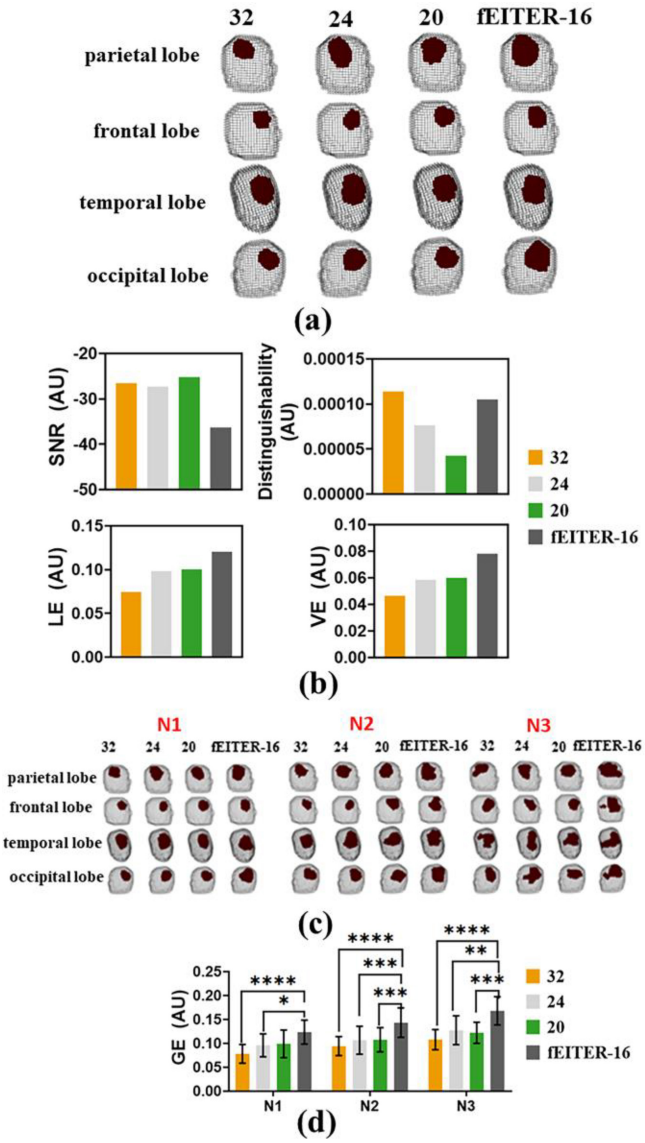

FIGURE 7. Quantitative and qualitative evaluations of different numbers of electrode configurations. The layout and driving strategy of the 32 electrodes configuration is a2 mode, with the measurement method being SKIP2. The 24 and 20 configurations predominantly inject current through nearly diameter electrodes at different heights, with measurement methods as SKIP1+AD and AD, respectively. 16 configuration is adopted by the fEITER system. (a) and (b) Reconstruction images and figures of merit (expressed as averages) without noise. (c) and (d) Reconstruction images and GE at various noise levels. (Images are presented as a 3-D model with RP. AU: Arbitrary unit.)

vertical resolution, providing potential clinical applications that can be enough sensitive to conductivity changes in the visual or somatosensory cortex. Therefore, we recommend the placement of electrodes in the suboccipital and central vertex regions for 3-D brain EIT, and the current should be injected through electrodes of varying heights as much as possible.

B. MEASUREMENT METHODS

Increasing the spacing between measurement channels will lead to an increase in the collected boundary voltage, which is desirable because the brain EIT signal becomes weak and limited due to the obstruction of the skull [39]. The exceptionally small potential changes are susceptible to external interference, rendering the measurement process more challenging and necessitating strict hardware parameter requirements. The simulation results reveal that SKIP modes can optimize signal evaluation metrics, albeit with a minor reduction in imaging quality, which is deemed acceptable in practical applications. Nonetheless, a more comprehensive quantitative comparison is needed to strike a balance between reconstruction error and signal quality for maximizing the benefits. This line of investigation falls outside the scope of the current study and warrants future exploration.

C. NUMBER OF ELECTRODES

The number of electrodes used in brain EIT should be given emphasis, given that this new imaging technology is primarily employed in acute brain injury monitoring and early warning in bedside or ambulance settings, with the advantage of being more convenient and cost-effective than CT and MRI scans [40]. Increasing the number of electrodes can significantly increase the number of independent measurements and obtain more impedance information, but it also entails higher costs and more time-consuming and labor-intensive operations. Moreover, in long-term monitoring, the occurrence rate of electrode detachment and displacement due to patient movements or fluid secretion is relatively high, resulting in measurement errors [41], [42]. Meanwhile, special populations, such as children, have limited surface area on their heads and cannot accommodate many electrodes [43]. However, insufficient electrodes can make it difficult to accurately obtain position or volume information of targets in the field, thereby reducing imaging accuracy. Therefore, it is necessary to select a reasonable number of electrodes that balance all factors. The 20-electrode configuration seems to be satisfactory, outperforming the 16-electrode configuration by far [Fig. 7(c) and (d)]. Although there is still a gap compared to the 32-electrode configuration, we believe that it already satisfies practical application requirements and should be tried first. However, if significant artifacts occur in the reconstruction that impairs the image's interpretation, more electrodes can be added.

D. LIMITATIONS AND PROSPECTS

In principle, the ideal research design for electrode configuration is to explore all possible scenarios and then use numerous simulation objectives and quantitative evaluation parameters for comparison and optimization. However, it is apparent that the potential number of arrangements in this work is vast, and the calculations are extremely complex, making it impractical. Therefore, we have adopted a specific approach, which summarizes the issues to be addressed in the electrode configuration into three categories, with each subsequent study building on the optimal solution of the previous one. While a perfect electrode configuration for 3-D brain EIT cannot be determined, it is encouraging that our study provides a valuable point of reference. Future methods,

which are more comprehensive, are likely to yield better results. Currently, we are considering conducting further physical model experiments.

V. CONCLUSION

Optimizing the layout and quantity of electrodes, driving protocols, and measurement modes is of practical significance for advancing the development of 3-D brain EIT.

Based on the findings of the simulation study in this article, further consideration of physical model experiments and human experiments is necessary to enhance our understanding of the optimal electrodes configuration, all of which will be conducted on a high-precision brain EIT data acquisition system [44]. Another promising avenue for exploration involves the arrangement of electrodes along high-conductivity skull suture structures, potentially enhancing current density within the brain tissue and consequently improving imaging accuracy [45].

REFERENCES

[1] F. Pennati et al., "Electrical impedance tomography: From the traditional design to the novel frontier of wearables," *Sensors*, vol. 23, no. 3, p. 1182, Jan. 2023.

[2] P. T. Cheung et al., "Electric impedance tomography enables portable and non-invasive approach to screen and monitor chronic kidney disease," in *Proc. Annu. Int. Conf. IEEE Eng. Med. Biol. Soc.*, 2023, pp. 1–4.

[3] G. Franchineau et al., "Electrical impedance tomography to monitor hypoxemic respiratory failure," *Am. J. Respir. Crit. Care Med.*, vol. 209, no. 6. pp. 670–682, Dec. 2023.

[4] J. H. W. Li et al., "Portable electrical impedance tomography (EIT) system stages non-alcoholic fatty liver disease for potential screening and monitoring at home," in *Proc. Annu. Int. Conf. IEEE Eng. Med. Biol. Soc.*, 2023, pp. 1–4.

[5] H. Lee, J. Culpepper, A. Farshkaran, B. McDermott, and E. Porter, "Impact of local electrodes on brain stroke type differentiation using electrical impedance tomography," in *Proc. Annu. Int. Conf. IEEE Eng. Med. Biol. Soc.*, 2021, pp. 1412–1415.

[6] X. Y. Ke et al., "Advances in electrical impedance tomography-based brain imaging," *Mil. Med. Res.*, vol. 9, no. 1, p. 10, Feb. 2022.

[7] X. Liu et al., "Fast iterative shrinkage-thresholding algorithm with continuation for brain injury monitoring imaging based on electrical impedance tomography," *Sensors*, vol. 22, no. 24, p. 9934, Dec. 2022.

[8] R. Wang, W. Zhu, G. Liang, J. Xu, J. Guo, and L. Wang, "Animal models for epileptic foci localization, seizure detection, and prediction by electrical impedance tomography," *Wiley Interdiscip. Rev. Cogn. Sci.*, vol. 13, no. 6, Nov. 2022, Art. no. e1619.

[9] J. Ma et al., "Exploratory study of a multifrequency EIT-based method for detecting intracranial abnormalities," *Front. Neurol.*, vol. 14, Aug. 2023, Art. no. 1210991.

[10] Y. Li et al., "Noninvasive cerebral imaging and monitoring using electrical impedance tomography during total aortic arch replacement," *J. Cardiothorac. Vasc. Anesth.*, vol. 32, no. 6, pp. 2469–2476, Dec. 2018.

[11] T. Tidswell, A. Gibson, R. H. Bayford, and D. S. Holder, "Three-dimensional electrical impedance tomography of human brain activity," *Neuroimage*, vol. 13, no. 2, pp. 283–94, Feb. 2001.

[12] M. Jehl, J. Avery, E. Malone, D. Holder, and T. Betcke, "Correcting electrode modelling errors in EIT on realistic 3D head models," *Physiol. Meas.*, vol. 36, no. 12, pp. 2423–42, Dec. 2015.

[13] J. Avery, K. Aristovich, B. Low, and D. Holder, "Reproducible 3D printed head tanks for electrical impedance tomography with realistic shape and conductivity distribution," *Physiol. Meas.*, vol. 38, no. 6, pp. 1116–1131, Jun. 2017.

[14] F. S. Moura, R. G. Beraldo, L. A. Ferreira, and S. Siltanen, "Anatomical atlas of the upper part of the human head for electroencephalography and bioimpedance applications," *Physiol. Meas.*, vol. 42, no. 10, Nov. 2021, Art. no. 105015.

[15] R. J. Sadleir and T. Tang, "Electrode configurations for detection of intraventricular haemorrhage in the premature neonate," *Physiol. Meas.*, vol. 30, no. 1, pp. 63–79, Jan. 2009.

[16] Y. Mamatjan, S. Ahn, T. Oh, and A. J. C. P. Adler, "Optimized electrode positions and stimulation patterns in head EIT," in *Proc. CMBES*, 2012, pp. 1–4.

[17] M. Faulkner, M. Jehl, K. Aristovich, J. Avery, A. Witkowska-Wrobel, and D. Holder, "Optimisation of current injection protocol based on a region of interest," *Physiol. Meas.*, vol. 38, no. 6, pp. 1158–1175, Jun. 2017.

[18] M. Fernandez-Corazza, S. Turovets, and C. H. Muravchik, "A novel bounded EIT protocol to generate inhomogeneous skull conductivity maps non-invasively," in *Proc. Annu. Int. Conf. IEEE Eng. Med. Biol. Soc.*, 2020, pp. 1440–1443.

[19] L. Fabrizi, A. McEwan, T. Oh, E. J. Woo, and D. S. Holder, "A comparison of two EIT systems suitable for imaging impedance changes in epilepsy," *Physiol. Meas.*, vol. 30, no. 6, pp. S103–120, Jun. 2009.

[20] L. Fabrizi, A. McEwan, T. Oh, E. J. Woo, and D. S. Holder, "An electrode addressing protocol for imaging brain function with electrical impedance tomography using a 16-channel semi-parallel system," *Physiol. Meas.*, vol. 30, no. 6, pp. S85–101, Jun 2009.

[21] T. Ouypornkochagorn, N. Terzija, P. Wright, J. L. Davidson, N. Polydorides, and H. McCann, "Scalp-mounted electrical impedance tomography of cerebral hemodynamics," *IEEE Sens. J.*, vol. 22, no. 5, pp. 4569–4580, Mar. 2022.

[22] T. Ouypornkochagorn, N. Polydorides, and H. McCann, "Towards continuous EIT monitoring for hemorrhagic stroke patients," *Front. Physiol.*, vol. 14, Apr. 2023, Art. no. 1157371.

[23] J. L. Davidson, P. Wright, S. T. Ahsan, R. L. Robinson, C. J. D. Pomfrett, and H. McCann, "fEITER–a new EIT instrument for functional brain imaging," *J. Phys., Conf. Ser.*, vol. 224, Apr. 2010, Art. no. 12025.

[24] L. L. Benzonana, N. J. S. Perry, and D. Ma, "Potential role of the PI3K pathway on renal cell carcinoma progression in vitro: Proceeding anaesthetic research society meeting," *Brit. J. Anaesth.*, vol. 106, no. 3, pp. 428P–446P, 2011.

[25] H. McCann, S. T. Ahsan, J. L. Davidson, R. L. Robinson, P. Wright, and C. J. Pomfrett, "A portable instrument for high-speed brain function imaging: FEITER," in *Proc. Annu. Int. Conf. IEEE Eng. Med. Biol. Soc.*, 2011, pp. 7029–7032.

[26] B. Packham et al., "Comparison of frequency difference reconstruction algorithms for the detection of acute stroke using EIT in a realistic head-shaped tank," *Physiol. Meas.*, vol. 33, no. 5, pp. 767–86, May 2012.

[27] S. Ahn, H. Wi, T. I. Oh, A. L. McEwan, S. C. Jun, and E. J. Woo, "Continuous nondestructive monitoring method using the reconstructed three-dimensional conductivity images via GREIT for tissue engineering," *J. Appl. Math.*, vol. 2014, pp. 1–11, Aug. 2014.

[28] B. Grychtol, B. Muller, and A. Adler, "3D EIT image reconstruction with GREIT," *Physiol. Meas.*, vol. 37, no. 6, pp. 785–800, Jun. 2016.

[29] J. Wagenaar and A. Adler, "Electrical impedance tomography in 3D using two electrode planes: Characterization and evaluation," *Physiol. Meas.*, vol. 37, no. 6, pp. 922–937, Jun. 2016.

[30] L. Horesh, "Some novel approaches in modelling and image reconstruction for multi-frequency electrical impedance tomography of the human brain," Ph.D. dissertation, Dept. Med. Phys., Univ. London, London, U.K., 2006.

[31] L. Fabrizi, L. Horesh, A. McEwan, and D. Holde, "A feasibility study for imaging of epileptic seizures by EIT using a realistic FEM of the head," in *Proc. World Congr. Med. Phys. Biomed. Eng.*, Seoul, South Korea, 2007, pp. 3874–3877.

[32] L. Yang et al., "The frequency spectral properties of electrode-skin contact impedance on human head and its frequency-dependent effects on frequency-difference EIT in stroke detection from 10Hz to 1MHz," *PLoS One*, vol. 12, no. 1, 2017, Art. no. e0170563.

[33] D. R. Akhmadullina, R. N. Konovalov, Y. A. Shpilyukova, E. Y. Fedotova, and S. N. Illarioshkin, "Anomia: Deciphering functional neuroanatomy in primary progressive aphasia variants," *Brain Sci.*, vol. 13, no. 12, p. 1703, Dec. 2023.

[34] R. T. Daley, H. J. Bowen, E. C. Fields, K. R. Parisi, A. Gutchess, and E. A. Kensinger, "Individual differences in older adult frontal lobe function relate to memory and neural activity for self-relevant and emotional content," *J. Gerontol. B Psychol. Sci. Soc. Sci.*, vol. 79, no. 3, Dec. 2023, Art. no. gbad186.

[35] Y. Jiang, X. Zhang, Z. Guo, and N. Jiang, "Altered functional connectivity during visual working memory state in patients with mild cognitive impairment," in *Proc. Annu. Int. Conf. IEEE Eng. Med. Biol. Soc.*, 2023, pp. 1–4.

[36] M. A. Nascimento et al., "Protracted neuronal recruitment in the temporal lobe of young children," *Nature*, vol. 626, pp. 1056–1065, Dec. 2023.

[37] B. M. Graham and A. Adler, "Electrode placement configurations for 3D EIT," *Physiol. Meas.*, vol. 28, no. 7, pp. S29–44, Jul. 2007.

[38] H. Li et al., "Unveiling the development of intracranial injury using dynamic brain EIT: An evaluation of current reconstruction algorithms," *Physiol. Meas.*, vol. 38, no. 9, pp. 1776–1790, Aug. 2017.

[39] Y. Shi, Y. Wu, M. Wang, Z. Tian, X. Kong, and X. He, "Sparse image reconstruction of intracerebral hemorrhage with electrical impedance tomography," *J. Med. Imag. (Bellingham)*, vol. 8, no. 1, Jan. 2021, Art. no. 014501.

[40] J. Ma et al., "Exploratory study on the methodology of fast imaging of unilateral stroke lesions by electrical impedance asymmetry in human heads," *Sci. World J.*, vol. 2014, May 2014, Art. no. 534012.

[41] M. A. Yokus and J. S. Jur, "Fabric-based wearable dry electrodes for body surface biopotential recording," *IEEE Trans. Biomed. Eng.*, vol. 63, no. 2, pp. 423–30, Feb. 2016.

[42] Y. Shi, Y. Lou, M. Wang, Z. Tian, B. Yang, and F. Fu, "A mismatch correction method for electrode offset in electrical impedance tomography," *IEEE Sensors J.*, vol. 22, no. 7, pp. 7248–7257, Apr. 2022.

[43] T. Tang, S. Oh, and R. J. Sadleir, "A robust current pattern for the detection of intraventricular hemorrhage in neonates using electrical impedance tomography," *Ann. Biomed. Eng.*, vol. 38, no. 8, pp. 2733–47, Aug. 2010.

[44] X. Shi et al., "High-precision electrical impedance tomography data acquisition system for brain imaging," *IEEE Sensors J.*, vol. 18, no. 14, pp. 5974–5984, Jul. 2018.

[45] C. Tang et al., "Correlation between structure and resistivity variations of the live human skull," *IEEE Trans. Biomed. Eng.*, vol. 55, no. 9, pp. 2286–2292, Sep. 2008.